Original Article

Comprehensive assessment of *in vivo* lumbar spine intervertebral discs using a 3D adiabatic $T_{1\rho}$ prepared ultrashort echo time (UTE-Adiab-$T_{1\rho}$) pulse sequence

Zhao Wei[1,2,3], Alecio F. Lombardi[1,4], Roland R. Lee[1], Mark Wallace[5], Koichi Masuda[6], Eric Y. Chang[1,4], Jiang Du[1], Graeme M. Bydder[1], Wenhui Yang[2,3], Ya-Jun Ma[1]

[1]Department of Radiology, University of California San Diego, La Jolla, CA, USA; [2]Institute of Electrical Engineering, Chinese Academy of Sciences, Beijing, China; [3]University of Chinese Academy of Sciences, Beijing, China; [4]Research Service, Veterans Affairs San Diego Healthcare System, La Jolla, CA, USA; [5]Department of Anesthesiology, University of California San Diego, La Jolla, CA, USA; [6]Department of Orthopedic Surgery, University of California San Diego, La Jolla, CA, USA

Contributions: (I) Conception and design: YJ Ma; (II) Administrative support: Z Wei, YJ Ma; (III) Provision of study materials or patients: Z Wei, YJ Ma; (IV) Collection and assembly of data: Z Wei; (V) Data analysis and interpretation: Z Wei, AF Lombardi; (VI) Manuscript writing: All authors; (VII) Final approval of manuscript: All authors.

Correspondence to: Ya-Jun Ma, PhD. Department of Radiology, University of California, San Diego, 9452 Medical Center Dr, La Jolla, CA 92037, USA. Email: yam013@ucsd.edu.

Background: $T_{1\rho}$ has been extensively reported as a sensitive biomarker of biochemical changes in the nucleus pulposus (NP) and annulus fibrosis of intervertebral discs (IVDs). However, no $T_{1\rho}$ study of cartilaginous endplates (CEPs) has yet been reported because the relatively long echo times (TEs) of conventional clinical $T_{1\rho}$ sequences cannot effectively capture the fast-decaying magnetic resonance signals of CEPs, which have very short T_2/T_2*s. This can be overcome by using ultrashort echo time (UTE) $T_{1\rho}$ acquisitions.

Methods: Seventeen subjects underwent UTE with adiabatic $T_{1\rho}$ preparation (UTE-Adiab-$T_{1\rho}$) and T_2-weighted fast spin echo imaging of their lumbar spines. Each IVD was manually segmented into seven regions (i.e., outer anterior annulus fibrosis, inner anterior annulus fibrosis, outer posterior annulus fibrosis, inner posterior annulus fibrosis, superior CEP, inferior CEP, and NP). $T_{1\rho}$ values of these sub-regions were correlated with IVD modified Pfirrmann grades and subjects' ages. In addition, $T_{1\rho}$ values were compared in subjects with and without low back pain (LBP).

Results: Correlations of $T_{1\rho}$ values of the outer posterior annulus fibrosis, superior CEP, inferior CEP, and NP with modified Pfirrmann grades were significant ($P<0.05$) with R values of 0.51, 0.36, 0.38, and −0.94, respectively. Correlations of $T_{1\rho}$ values of the outer anterior annulus fibrosis, outer posterior annulus fibrosis, and NP with ages were significant with R equal to 0.52, 0.71, and −0.76, respectively. $T_{1\rho}$ differences of the outer posterior annulus fibrosis, inferior CEP, and NP between the subjects with and without LBP were significant ($P=0.005$, 0.020, and 0.000, respectively).

Conclusions: The UTE-Adiab-$T_{1\rho}$ sequence can quantify $T_{1\rho}$ of whole IVDs including CEPs. This is an advance, and of value for comprehensive assessment of IVD degeneration.

Keywords: Magnetic resonance imaging (MRI); low back pain (LBP); disc degeneration; ultrashort echo time (UTE); adiabatic $T_{1\rho}$

Submitted Mar 20, 2021. Accepted for publication May 19, 2021.
doi: 10.21037/qims-21-308
View this article at: https://dx.doi.org/10.21037/qims-21-308

Introduction

Low back pain (LBP) is a leading cause of disability in adults in the United States with socio-economic costs of the condition estimated at $100 billion annually (1,2). Though the precise etiology of LBP is not fully understood, intervertebral disc (IVD) degeneration is recognized as one of the major contributors to the condition (3-6).

The healthy IVD has a distinct morphological and biochemical composition: its central nucleus pulposus (NP) is a gelatinous core of proteoglycans and water, its peripheral annulus fibrosus (AF) consists of a series of concentric rings of lamellae type-1 collagen fibers, and the cartilaginous endplate (CEP) is a thin layer of hyaline-like cartilage on either side of the IVD. The CEP is adjacent to the vertebral bodies above and below IVDs (7). With aging and degeneration, the IVD undergoes changes to its morphology and biochemistry including proteoglycan loss, dehydration, CEP degradation, loss of disc height, annular tears, and extrusion (8-10).

Magnetic resonance imaging (MRI) is widely used in clinical practice to image lumbar IVDs (11). Conventional MRI sequences, such as the T_2-weighted fast spin echo (T_2w-FSE), are highly effective for evaluating IVD morphological changes. However, these sequences are not normally used to quantify the effects of biochemical changes in IVDs, which limits their sensitivity and specificity in the assessment of IVD degeneration, especially in the early stages of this condition. Quantitative MRI techniques, including measurement of T_2, $T_{1\rho}$, magnetization transfer, and diffusion metrics, offer promising avenues for this purpose (12). Among them, $T_{1\rho}$ describes spin-lattice relaxation in the rotating frame in the presence of an external spin-lock RF pulse. $T_{1\rho}$ is a unique biomarker that reflects low frequency motional biological processes including those arising from macromolecule–water interactions, such as those between proteoglycans and water, when the strength of the locking RF pulse is properly set (13,14). Many studies have demonstrated that quantitative $T_{1\rho}$ mapping is a promising technique for detecting biochemical changes in IVDs during the process of degeneration (14-18). To date, research on $T_{1\rho}$ measurements of IVDs has focused on changes in the NP (16,18-22), and the AF (20-22). The CEP may be degraded, affecting nutrient availability and cell metabolism in the remainder of the IVD and, thus, contribute to degeneration of the NP and AF (9). To the best of our knowledge, only one $T_{1\rho}$ measurement study of the CEP has been performed to evaluate its normal state, change with age and contribution to IVD degeneration (23). This is because conventional clinical sequences, such as gradient recalled echo and FSE sequences, with relatively long echo times (TEs) cannot capture the fast decaying MR signal from the CEP with a short T_2 relaxation time (24).

To address this problem, we propose the use of a three-dimensional (3D) ultrashort TE sequence with adiabatic $T_{1\rho}$ preparation (UTE-Adiab-$T_{1\rho}$), which can provide $T_{1\rho}$ mapping of the entire lumbar IVD, including the CEP (25). The TE of the UTE-Adiab-$T_{1\rho}$ sequence can be as short as 32 μs (25), and signals from both long T_2 tissues in the disc (e.g., the NP and inner AF) as well as very short T_2 tissues (e.g., the CEP) (26) can be detected by this sequence. Moreover, the Adiab-$T_{1\rho}$ preparation is much less sensitive to the magic angle effect than conventional continuous-wave $T_{1\rho}$ preparations (25,27-29). This is an important feature of the proposed UTE-Adiab-$T_{1\rho}$ sequence because collagen fibers in both the AF and CEP are highly ordered and have different orientations to the main magnetic field (i.e., B0). This can result in different degrees of magic angle effect with confounding changes in measured T_2/T_2* values that are unrelated to disease (24,30).

The CEP is a barrier that resists disc pressure and provides a gateway for the transport of disc nutrients and metabolites. Quantitative $T_{1\rho}$ measurement to study the relationship between CEP dysfunction and IVD degeneration has only been possible following the introduction of the UTE method to image the CEP (24,30,31). This may also provide valuable research options in the future. In this feasibility study, 17 human subjects (mean age ± standard deviation: 43±16 years; range: 25–71 years; 9 women, 8 men) were recruited. Each lumbar IVD was manually segmented into seven sub-regions [i.e., outer anterior AF (OAAF), inner anterior AF (IAAF), outer posterior AF (OPAF), inner posterior AF (IPAF), superior CEP (SCEP), inferior CEP (ICEP), and NP]. The $T_{1\rho}$ values of these sub-regions were correlated with modified Pfirrmann grades and subjects' ages. In addition, $T_{1\rho}$ value differences between subjects with and without LBP (No-LBP) were compared.

Methods

All scans were performed on a 3T clinical MRI scanner (MR750, GE Healthcare Technology, Milwaukee, WI, USA). A four-channel phased array spine coil was used for signal reception (the body coil was used for signal excitation). In our study, only two channels covering the

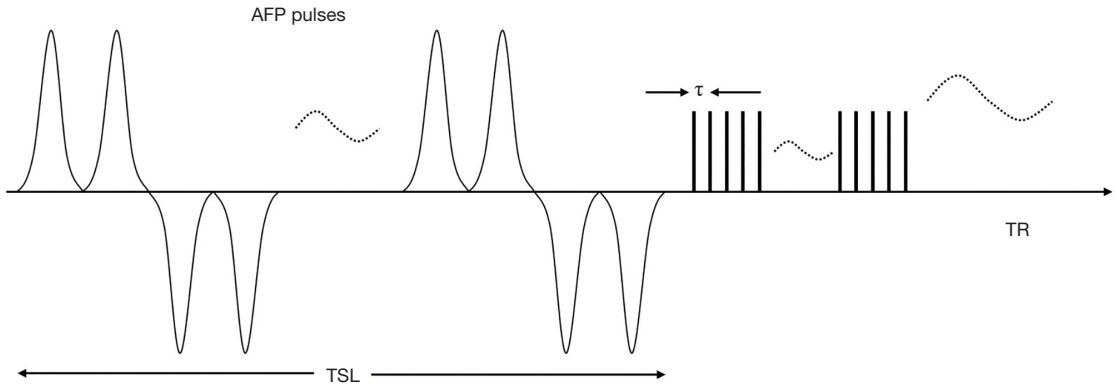

Figure 1 Diagram of the 3D UTE-Adiab-$T_{1\rho}$ sequence. A train of adiabatic full passage preparation pulses is used to generate $T_{1\rho}$ contrast during the period TSL. This is followed by multiple 3D UTE data acquisition spokes separated by time τ. The cycle is repeated every TR. UTE-Adiab-$T_{1\rho}$, ultrashort echo time sequence with adiabatic $T_{1\rho}$ preparation; AFP, adiabatic full passage; TSL, spin lock time; TR, repetition time.

lumbar spine region were activated during the scan. A 5 s calibration scan was performed to correct the signal variation in the clinical images induced by inhomogeneous coil sensitivity.

Subjects

The study received Institutional Review Board approval and written informed consents were obtained from all participants. The study was conducted in accordance with the Declaration of Helsinki (as revised in 2013). From December 2019 to March 2020, a total of 17 participants (mean age ± standard deviation: 43±16 years; range: 25–71 years; 9 women, 8 men) recruited by use of a study flyer met the inclusion criteria. The inclusion criteria specified that participants must be actively walking, be between ages 18 and 90 years, have no LBP or have experienced a single or recurrent episodes of LBP. Exclusion criteria were previous spine surgery, traumatic lumbar spine injury, spine tumor, infectious spine lesion, contraindications to MR imaging, radicular pain, and neurologic deficits of the lower limbs in the past six months. No participants recruited were subject to the exclusion criteria. Six participants (mean age ± standard deviation: 60±13 years; range: 38–71 years; 2 women, 4 men) reported LBP.

MRI pulse sequences

Key features of the 3D UTE-Adiab-$T_{1\rho}$ sequence are shown in *Figure 1*. A set of spin-locking preparations containing an even number of adiabatic full passage pulses is followed by multiple 3D UTE acquisition spokes with an equal time interval τ between them to provide fast data acquisition (25). A 3D Cones trajectory is used for UTE spatial encoding during the data acquisition (32). Spin lock time is defined as the total duration of the train of adiabatic full passage pulses (i.e., spin lock time equals to the product of the duration of a single adiabatic full passage pulse and the number of adiabatic full passage pulses). Repetition time (TR) is the time between sequential adiabatic $T_{1\rho}$ preparations. The 3D k-space data was regridded with a Kaiser-Bessel kernel. After Fourier transform, the final UTE images were produced by multichannel image combination using a sum-of-squares method.

The signal S(TSL) at the acquisition time is given by:

$$S(TSL) = S_0 e^{-\frac{TSL}{T_{1\rho}}} + C \quad [1]$$

where S_0 is the initial signal intensity, TSL is the spin lock time, and C is a constant describing non-$T_{1\rho}$ related signals, such as the background noise and artifacts generated during data acquisition and image reconstruction (25).

Numerical simulations were conducted to determine optimized sequence parameters for *in vivo* studies. The final sequence parameters used in the *in vivo* study were: TR =2,000 ms, flip angle =6°, and number of spokes =41. More details about simulation studies and the corresponding results can be found in the Supplemental Material for this paper (Appendix 1).

Both 3D UTE-Adiab-$T_{1\rho}$ and clinical 2D T_2w-FSE

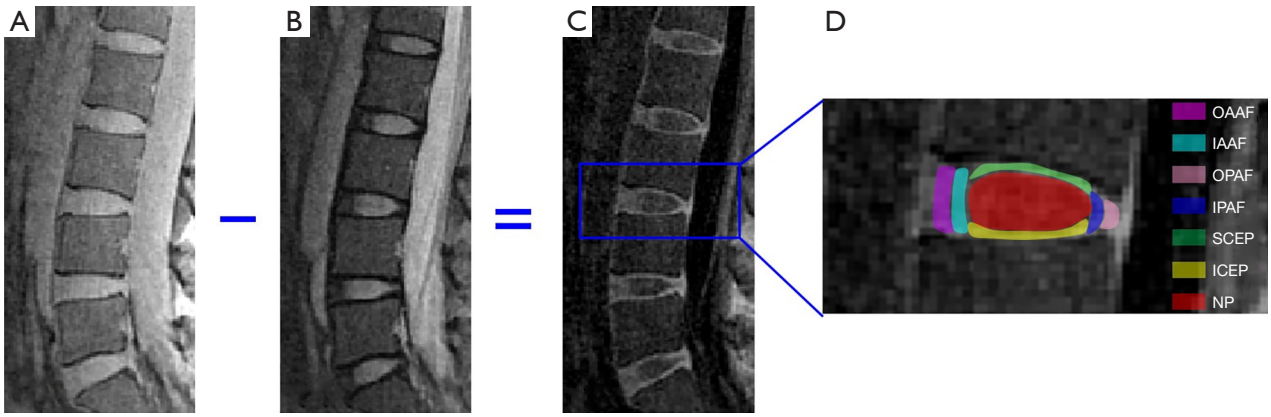

Figure 2 Disc segmentation. Sagittal lumbar spine UTE-Adiab-$T_{1\rho}$ images are shown with TSLs of 0 (A) and 69.12 (B) ms; (C) shows subtraction of (B) from (A), which highlights the CEP and allows better segmentation; (D) shows the seven ROIs within a disc. UTE-Adiab-$T_{1\rho}$, ultrashort echo time sequence with adiabatic $T_{1\rho}$ preparation; TSL, spin lock time; OAAF, outer anterior annulus fibrosus (AF); IAAF, inner anterior AF; OPAF, outer posterior AF; IPAF, inner posterior AF; SCEP, superior cartilaginous endplate (CEP); ICEP, inferior CEP; NP, nucleus pulposus.

sequences were used in the sagittal plane to scan the lumbar spine of each subject in the study. The sequence parameters were: (I) UTE-Adiab-$T_{1\rho}$ sequences: bandwidth of the adiabatic pulse =1,150 Hz, peak amplitude of the adiabatic pulse =12 μT, number of adiabatic full passage pulses =0, 4, 8, and 12, duration of a single adiabatic full passage pulse =8.64 ms, τ =5 ms, TE =0.1 ms (the minimum TE is limited by the transmitter and receiver switching time as well as the coil ring down time), TR =2,000 ms, flip angle =6°, field of view =280×280×56 mm^3, matrix =320×320×14, bandwidth =250 kHz, spin lock time =0, 34.56, 69.12, and 103.68 ms, number of spokes =41, total scan time =17 min 36 s; (II) T_2w-FSE sequence: TE =102 ms, TR =4,041 ms, slice thickness =3.5 mm, field of view =340×340 mm^2, matrix =384×384, bandwidth =250 kHz, slice number =14, scan time =1 min 50 s.

$T_{1\rho}$ calculation and disc segmentation

To correct for subject inter-scan motion during scan, 3D non-rigid motion registration was performed on the UTE-Adiab-$T_{1\rho}$ images with the Elastix software using both affine and B-spline transformation (33,34). Quantitative $T_{1\rho}$ maps of the five lumbar IVDs (i.e., L1/L2 to L5/S1) visualized in each subject were generated offline with Matlab 2018b (MathsWork Inc, Natick, MA, USA). The Levenberg-Marquardt algorithm was used to provide nonlinear fitting of Eq. [1] using images acquired with the 3D UTE-Adiab-$T_{1\rho}$ sequences. Before data fitting, the 3D UTE-Adiab-$T_{1\rho}$ images were smoothed with a 3D Gaussian filter (kernel size 3×3×3 and standard deviation 0.6) to improve image SNR for more accurate $T_{1\rho}$ quantification.

A total of 85 IVDs from the 17 subjects were analyzed. Each IVD was manually segmented into seven regions (i.e., OAAF, IAAF, OPAF, IPAF, SCEP, ICEP, and NP) by two observers (a musculoskeletal radiologist with seven years' experience and a trained PhD student), as shown in *Figure 2*. Regions of interest (ROIs) from each sub-region were drawn on subtraction images (second image subtracted from the first) obtained from $T_{1\rho}$ weighted images with spin lock times =0 and 69.12 ms. These were copied and pasted onto the original $T_{1\rho}$ weighted images to allow fitting of the $T_{1\rho}$ data. As can be seen in *Figure 2*, the CEP is highlighted on the subtraction image. This demonstrates the feasibility of imaging the CEP and providing data about it for quantification using the 3D UTE-Adiab-$T_{1\rho}$ sequence. For each IVD, the $T_{1\rho}$ value of each sub-region was averaged from five or six central sagittal slices.

IVD degeneration grading

The 85 discs were graded independently by two observers (same as aforementioned) using the modified Pfirrmann system. This is a widely used method of determining the degree of disc degeneration through qualitative assessment of the morphology and signal intensity of the NP and AF using clinical T_2w-FSE images (35). The number of discs in each grade is shown in *Table 1*.

Table 1 The P value of the Spearman's correlation coefficient between the $T_{1\rho}$ value and the modified Pfirrmann grade within each sub-region of the IVD

Grade	Number of discs	$T_{1\rho}$ (ms)						
		OAAF	IAAF	OPAF	IPAF	SCEP	ICEP	NP
2	31 (36.5%)	33.2±7.8	44.9±7.7	34.0±5.0	45.4±6.5	36.0±5.0	36.9±3.9	118.7±10.9
3	12 (14.1%)	31.2±7.0	43.9±7.9	34.1±4.5	45.5±7.5	40.9±6.8	40.5±4.7	102.4±5.5
4	9 (10.6%)	34.9±5.7	45.2±5.4	35.5±4.6	46.6±8.0	35.6±4.3	37.3±5.6	84.5±11.1
5	7 (8.2%)	34.2±7.1	45.4±4.9	39.0±6.5	46.5±6.8	39.3±5.4	38.5±2.7	76.4±2.4
6	11 (12.9%)	34.8±6.8	44.6±4.6	41.9±7.7	48.1±6.3	38.5±2.6	40.8±3.5	68.0±3.0
7	12 (14.1%)	36.6±5.5	44.4±4.0	40.8±5.3	47.5±7.4	42.5±4.5	42.0±5.1	59.9±7.7
8	3 (3.5%)	32.4±7.3	36.5± 8.4	41.8±5.2	46.3±6.1	43.5±5.6	42.5±4.9	49.7±3.1
P value		0.132	0.726	0.000*	0.385	0.000*	0.001*	0.000*

The $T_{1\rho}$ values were described as means ± standard deviations. *P<0.05, significant correlation. The subjects were divided into 7 groups according to the modified Pfirrmann grade. No IVD was classified as Grade 1. IVD, intervertebral disc; OAAF, outer anterior annulus fibrosus (AF); IAAF, inner anterior AF; OPAF, outer posterior AF; IPAF, inner posterior AF; SCEP, superior cartilaginous endplate (CEP); ICEP, inferior CEP; NP, nucleus pulposus.

Statistical analysis

All statistical analyses were performed using SPSS (Version 24.0, IBM SPSS, Chicago, IL, USA). To test the inter-observer reproducibility for the ROI segmentation, intra- and interclass correlation coefficients (ICCs) with 95% confidence intervals were calculated to evaluate the inter-agreement of $T_{1\rho}$ values of all the ROIs for the two observers. An ICC >0.90 was considered excellent agreement. The agreement of modified Pfirrmann grades between observers was evaluated with Cohen's Kappa analysis. The correlations between $T_{1\rho}$ values of sub-regions and the corresponding modified Pfirrmann grades of IVDs as well as subjects' ages were analyzed with Spearman's Rank Order Correlation. For each sub-region, $T_{1\rho}$ values between different grades were compared using the one-way analysis of variance (ANOVA) method. Finally, $T_{1\rho}$ differences between subjects with and without LBP were evaluated using Student's *t*-test.

Results

Representative $T_{1\rho}$ fitting curves of the OAAF, SCEP, and NP are shown in *Figure 3*. The ICCs of $T_{1\rho}$ values of the OAAF, IAAF, OPAF, IPAF, SCEP, ICEP, and NP between the two observers were 0.97, 0.94, 0.95, 0.90, 0.96, 0.91, and 0.97, respectively. In addition, the Kappa value between the modified Pfirrmann grades given by the two observers was 0.81. These results demonstrate good inter-observer reproducibility for both ROI segmentation and modified Pfirmann grading.

Figure 4 shows representative $T_{1\rho}$ maps of lumbar IVDs from four subjects, with the corresponding clinical T_2w-FSE images. These images demonstrate that the UTE-Adiab-$T_{1\rho}$ sequence can be used to measure $T_{1\rho}$ values of the whole IVD, including the CEP. In comparison, the CEP regions showed very low signal and their signals were not distinguishable from noise on the T_2w-FSE images. As can be seen in *Figure 4*, more degraded discs with higher modified Pfirrmann grades (*Figure 4E-4H*) generally showed lower $T_{1\rho}$ values in NPs (*Figure 4A-4D*).

The $T_{1\rho}$ values of IVDs and the number of discs in each grade (using modified Pfirrmann grades) are summarized in *Table 1*. Spearman's analysis showed that correlations between $T_{1\rho}$ values of the OPAF, SCEP, ICEP, and NP and modified Pfirrmann grades were significant (P<0.05). $T_{1\rho}$ values of the OPAF, SCEP, and ICEP showed moderate positive correlations with grades with R equal to 0.51, 0.36, and 0.38, respectively. In contrast, the $T_{1\rho}$ of the NP was inversely correlated with grades with an R of –0.94, which is consistent with reported trends for the NP (16,18,19). The corresponding scatter plots of $T_{1\rho}$ values for the OPAF, SCEP, ICEP, and NP as a function of the modified Pfirrmann grade are shown in *Figure 5*.

Because the sample sizes of the modified Pfirrmann grades 4 (n=9), 5 (n=7), and 8 (n=3) were too small to be

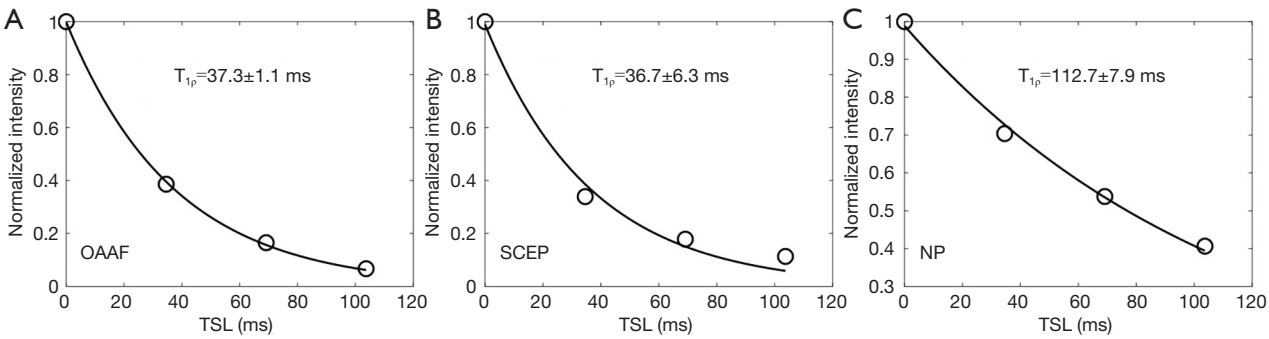

Figure 3 Representative $T_{1\rho}$ fitting curves of three sub-regions (i.e., OAAF, SCEP and NP) within a disc in a healthy 37-year-old male subject. Intensity shown along the y-axis is normalized by the maximum signals of the four UTE-Adiab-$T_{1\rho}$ data. The Levenberg-Marquardt algorithm was used to provide nonlinear fitting. OAAF, outer anterior annulus fibrosus; SCEP, superior cartilaginous endplate; NP, nucleus pulposus.

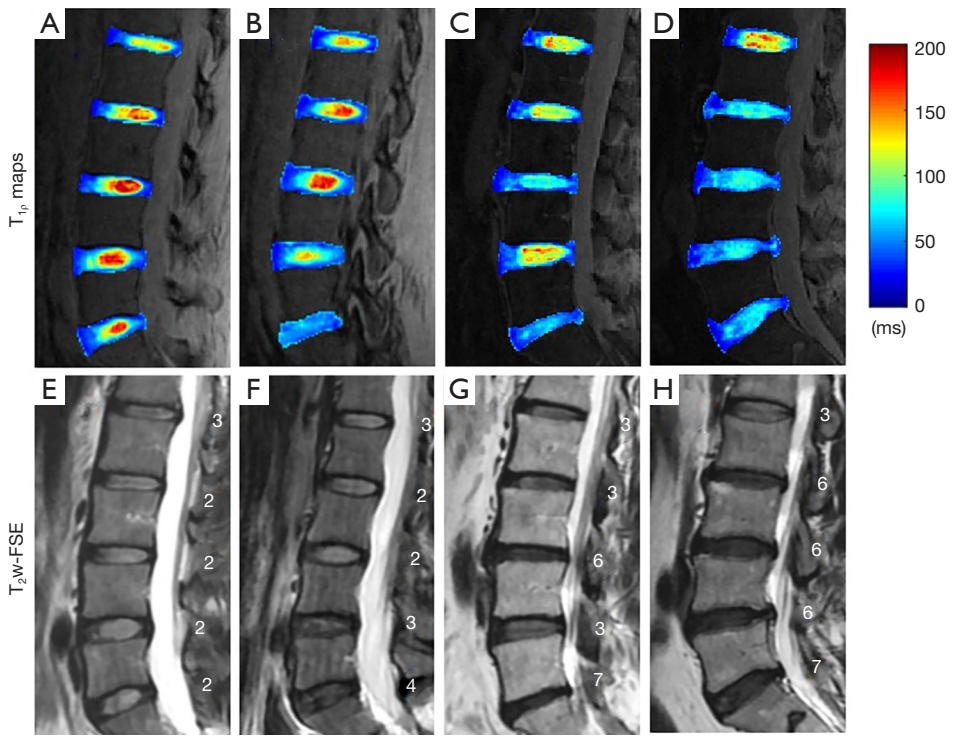

Figure 4 Representative $T_{1\rho}$ maps (first row) and corresponding T_2w-FSE images (second row) from four subjects (first column, 29-year-old woman; sond column, 32-year-old woman; third column, 60-year-old woman; fourth column, 55-year-old man). The modified Pfirrmann grades for each disc are shown on the T_2w-FSE images. T_2w-FSE, T_2 weighted fast spin echo.

treated as independent groups, the discs were classified into four separate groups by grade (i.e., group 1: grade 2; group 2: grades 3 and 4; group 3: grades 5 and 6; group 4: grades 7 and 8). $T_{1\rho}$ values of the seven sub-regions in each group and the corresponding ANOVA analysis results can be found in Tables S1,S2, respectively. Representative bar plots for the OPAF, SCEP, ICEP, and NP are shown in *Figure 6*. In the NP, $T_{1\rho}$ differences between every pair of groups were significant. $T_{1\rho}$ values of group 4 in the OPAF, SCEP, and ICEP showed significant differences compared with

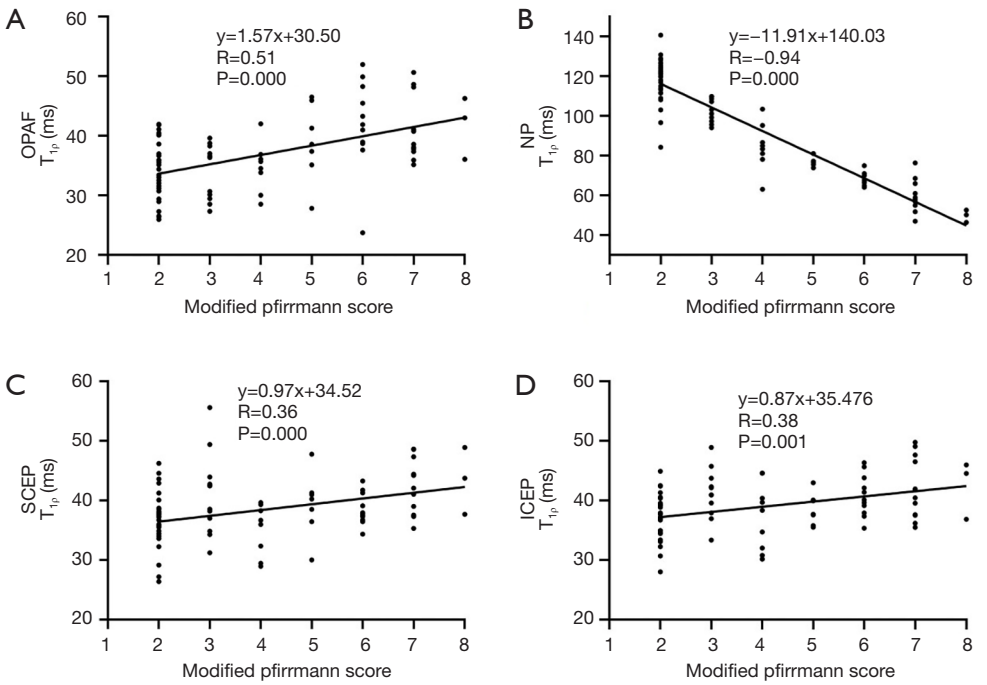

Figure 5 Spearman's correlation coefficients between modified Pfirrmann grades and $T_{1\rho}$ values of OPAF (A), SCEP (B), ICEP (C), and NP (D). A strong negative correlation is observed for the NP, and moderate positive correlations are observed for the OPAF, SCEP, and ICEP. OPAF, outer posterior annulus fibrosus; SCEP, superior cartilaginous endplate (CEP); ICEP, inferior CEP; NP, nucleus pulposus.

the $T_{1\rho}$ of groups 1 and 2 (P<0.05). $T_{1\rho}$ differences between group 3 and groups 1 and 2 in the OPAF, group 3 and group 4 in the SCEP, and group 1 and group 3 in the ICEP were significant.

The $T_{1\rho}$ values of the OAAF and OPAF showed positive correlations with ages (R=0.52 and 0.71, respectively), and the $T_{1\rho}$ value of the NP showed an inverse correlation with age (R=−0.76), consistent with the trend reported in reference (14). The corresponding scatter plots of $T_{1\rho}$ values of the OAAF, OPAF, and NP as a function of the age can be found in Figure S2.

As can be seen in *Table 2*, $T_{1\rho}$ differences of the OPAF, ICEP, and NP between the LBP and No-LBP groups were significant (P=0.005, 0.020, and 0.000, respectively). As shown in *Figure* 7, the mean $T_{1\rho}$ values of the OPAF and ICEP in all the subjects with LBP were greater than those without LBP, while the mean $T_{1\rho}$ of the NP of those subjects with LBP was lower.

Discussion

The study demonstrates the feasibility of using the 3D UTE-Adiab-$T_{1\rho}$ sequence to measure the $T_{1\rho}$ of an entire lumbar IVD, especially of the CEP. The sequence can capture very short T_2 CEP signals and has the advantage of being less sensitive to the magic angle effect than the conventional continuous-wave $T_{1\rho}$ method (25,27-29). With images acquired with the 3D UTE-Adiab-$T_{1\rho}$ technique, $T_{1\rho}$ maps of entire lumbar IVDs were generated for 17 subjects. The $T_{1\rho}$ of the NP showed a significant negative correlation with the modified Pfirrmann grade (R=−0.94). $T_{1\rho}$ values of the OPAF, SCEP, and ICEP showed moderate positive correlations with the modified Pfirrmann grade (R=0.51, 0.36, and 0.38, respectively). $T_{1\rho}$ values of the NP and OPAF also showed significant correlations with age (R=−0.76 and 0.71, respectively), and the $T_{1\rho}$ value of the OAAF showed a moderate correlation with age (R=0.52). $T_{1\rho}$ value differences of the OPAF, ICEP, and NP between LBP and No-LBP groups were significant (P=0.005, 0.020, and 0.000, respectively). These findings indicate that the UTE-Adiab-$T_{1\rho}$ technique has considerable potential for the comprehensive assessment of IVD degeneration.

The $T_{1\rho}$ value changes with different modified Pfirrmann grades may reflect biochemical composition differences during degeneration in the lumbar IVD. As with previous studies, the inverse correlation between the $T_{1\rho}$ of the

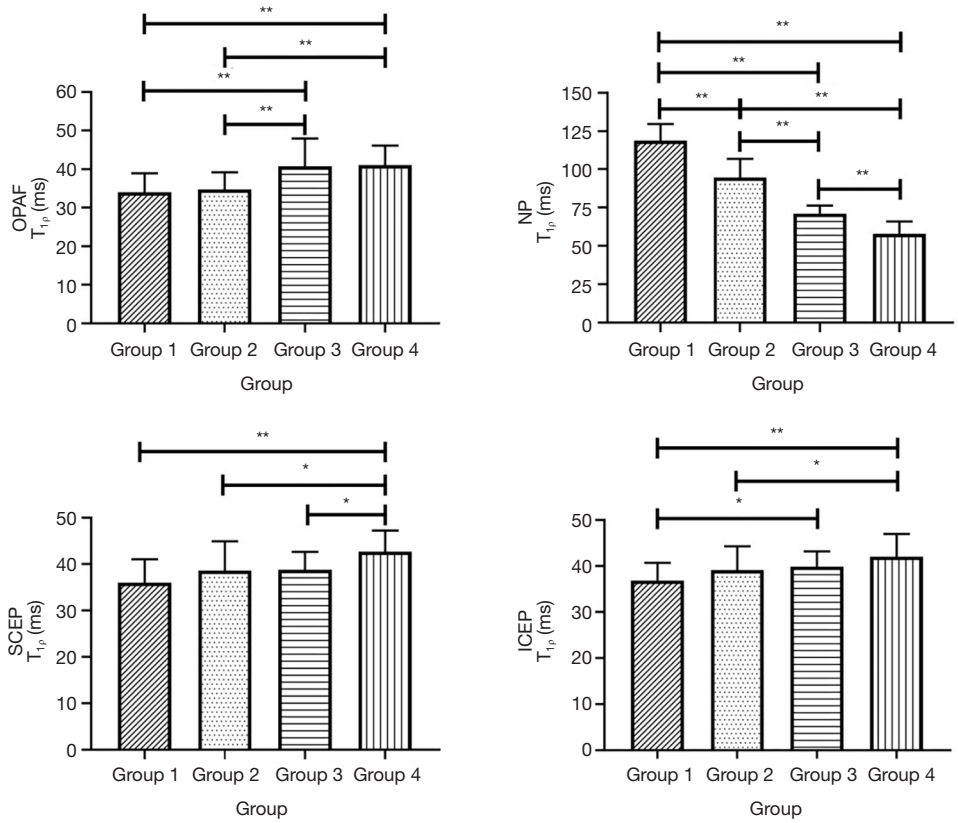

Figure 6 Mean $T_{1\rho}$ values of the OPAF, SCEP, ICEP, and NP regions for four different modified Pfirrmann grade groups (i.e., group 1: grade 2; group 2: grades 3 and 4; group 3: grades 5 and 6; group 4: grades 7 and 8), respectively. *, P<0.05; **, P<0.01. OPAF, outer posterior annulus fibrosus; SCEP, superior cartilaginous endplate (CEP); ICEP, inferior CEP; NP, nucleus pulposus.

NP and the modified Pfirrmann grade may reflect loss of proteoglycans during the process of degeneration (18-21). The $T_{1\rho}$ of the OPAF showed a positive correlation with the modified Pfirrmann grade, consistent with loss of collagen integrity in the OPAF region during IVD degeneration. This trend can also be seen in representative $T_{1\rho}$ maps of IVDs in *Figure 4*. The OPAF regions of IVDs with higher grades (e.g., L2/L3~L5/S1 in *Figure 4D*) show greater $T_{1\rho}$ values than IVDs with lower grades (e.g., L2/L3~L5/S1 in *Figure 4A*). This may be because a portion of the proteoglycans of the NP "spread" into the OPAF as a result of compression during the process of degeneration. However, the positive correlations between $T_{1\rho}$ values of the SCEP and ICEP and modified Pfirrmann grades imply a proteoglycan content decrease during the disc degeneration. This finding is in agreement with Sarma's study, in which the authors found that $T_{1\rho}$ values increased almost linearly with proteoglycan depletion in cartilage (36). Our results demonstrate that $T_{1\rho}$ values of the OPAF, SCEP, ICEP, and NP may be useful indicators of lumbar IVD degeneration.

The good correlations between $T_{1\rho}$ values of the OAAF, OPAF, and NP and age imply that the UTE-Adiab-$T_{1\rho}$ measurements of these sub-regions may be valuable indicators of age-related disc degeneration. In addition, $T_{1\rho}$ values of the OPAF, ICEP, and NP may provide information about the mechanism of LBP since these $T_{1\rho}$ values showed significant differences between the LBP and No-LBP groups.

There are very few studies that measure the T_2 and $T_{1\rho}$ values of the CEP. Ling *et al.* reported that both T_2 and $T_{1\rho}$ values of the CEP were around 30 ms in a 1.5T study (23). Cao *et al.* reported an unexpectedly high value of T_2 in the CEP which was around 60 ms (37). This could have been caused by partial volume effects since their spatial resolution was quite low. T_2* values of CEPs measured using UTE sequences were around 15 ms (24,30). In our

Table 2 P values of $T_{1\rho}$ differences comparison between LBP and No-LBP groups (P-LBP) and P values of correlation analysis between the $T_{1\rho}$ value and age (P-Age), within sub-region of the IVD

Group	Number	Age (years)	$T_{1\rho}$ (ms)			
			OAAF	OPAF	ICEP	NP
LBP	#1	70	37.6±4.6	39.6±4.9	42.4±6.5	65.1±8.0
	#2	38	29.4±3.2	38.5±1.9	38.7±2.2	63.5±14.3
	#3	71	39.7±4.8	44.3±6.9	43.2±2.2	74.3±9.8
	#4	55	29.8±4.3	40.4±2.4	38.7±2.5	75.2±18.4
	#5	57	36.5±3.6	43.4±6.8	45.2±1.8	72.9±21.1
	#6	71	38.9±2.7	41.2±6.2	41.9±4.1	59.0±8.9
	Mean		35.3±4.6	41.2±2.2	41.7±3.2	68.3±6.7
No-LBP	#7	29	36.0±3.0	38.3±2.7	42.2±2.3	117.6±8.4
	#8	32	36.4±5.7	33.6±3.6	34.6±1.5	97.9±22.3
	#9	35	32.3±4.0	33.7±2.9	34.2±4.1	95.5±19.7
	#10	27	23.4±2.3	28.3±2.1	42.5±4.7	95.0±6.4
	#11	37	32.8±4.5	32.5±2.9	35.2±4.0	115.7±17.9
	#12	60	38.3±6.3	38.0±1.2	41.0±1.8	88.1±21.6
	#13	35	44.8±3.7	39.3±2.9	39.2±2.1	117.6±6.4
	#14	29	27.3±2.0	36.3±5.3	38.9±2.6	110.1±33.2
	#15	25	22.4±2.4	27.7±3.4	32.8±3.8	97.2±25.1
	#16	38	39.3±4.3	41.8±4.3	35.0±1.9	104.8±28.0
	#17	32	30.1±1.6	29.2±2.5	37.1±2.3	114.3±10.0
	Mean		33.0±6.9	34.4±4.7	37.5±3.4	104.9±10.6
P-LBP			0.480	0.005*	0.020*	0.000*
P-Age			0.004*	0.000*	0.087	0.004*

The $T_{1\rho}$ values are described as means±standard deviations. The $T_{1\rho}$ value for a subject is the average of the five lumbar intervertebral discs. *P<0.05, significant difference/correlation. IVD, intervertebral disc; LBP, low back pain; No-LBP, without low back pain; OAAF, outer anterior annulus fibrosus (AF); OPAF, outer posterior AF; ICEP, inferior cartilaginous endplate; NP, nucleus pulposus.

study, the CEP $T_{1\rho}$ values ranged from 30 to 45 ms, which is higher than the previously reported T_2* values. The CEP may contain both short and long T_2 water components. Multi-compartment $T_{1\rho}$ quantification is interesting and could be done with either a continuous wave prepared UTE sequence or a UTE-Adiab-$T_{1\rho}$ sequence using different TEs (e.g., 0.1 *vs.* 2–3 ms) (38).

Following each Adiab-$T_{1\rho}$ preparation, 41 UTE spokes were acquired to speed up the data acquisition. However, this long train of spokes can introduce signal variation along the spokes in a single TR, which may affect the image quality. A variable flip angle design may solve this problem which will be studied in future.

The image resolution of our UTE-Adiab-$T_{1\rho}$ sequence is relatively low compared to the thickness of the CEP (i.e., approximately 0.6–1.0 mm). There is always a trade-off between spatial resolution, scan time, and image SNR. We expect a more advanced RF coil with higher SNR performance will be available in future to allow improvement of spatial resolution without compromise of scan time or SNR.

There are several limitations to this study. First, the sample size was relatively small and designed to assess technical feasibility rather than clinical utility. A future

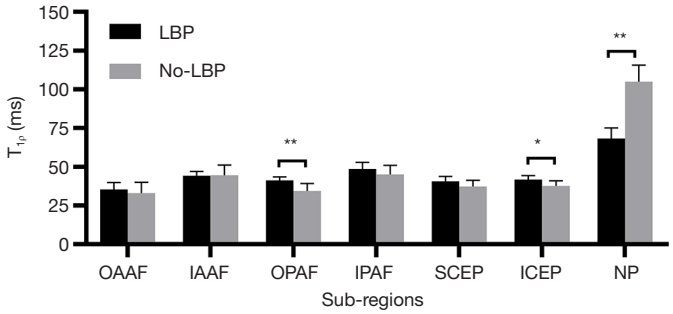

Figure 7 Mean $T_{1\rho}$ values of the seven sub-regions in the LBP and No-LBP groups. Significant differences between the two groups are seen for the NP, ICEP and OPAF regions. *, P<0.05; **, P<0.01. LBP, low back pain; No-LBP, without LBP; OAAF, outer anterior annulus fibrosus (AF); IAAF, inner anterior AF; OPAF, outer posterior AF; IPAF, inner posterior AF; SCEP, superior cartilaginous endplate (CEP); ICEP, inferior CEP; NP, nucleus pulposus.

study with more subjects will be conducted. Second, no biochemical or histological validation was performed in this study. This could be included in the future, using fresh cadaveric specimens. Third, the scan time of the $T_{1\rho}$ measurement protocol with four UTE-Adiab-$T_{1\rho}$ sequences was about 17 min, which is long for use in the clinical practice. Advanced acceleration techniques including compressed sensing and deep learning can be used to address this problem (39,40). $T_{1\rho}$ values may vary with different types of sequence. It would not be surprising if UTE quantification shows similar differences since UTE sequences detect signals from both short and long T_2 components while clinical sequences only image long T_2 components. In general, comparisons should be conducted with similar sequences, although this may be challenging with studies performed using different vendors' systems.

Conclusions

The 3D UTE-Adiab-$T_{1\rho}$ technique provides volumetric $T_{1\rho}$ mapping of the entire IVD, especially of the CEP. This provides comprehensive assessment of IVD degeneration and may improve understanding of the origin of LBP.

Acknowledgments

Funding: This work was supported by National Institutes of Health (R01AR075825 to EC, R01AR062581 to JD, R01AR068987 to JD, R21AR075851 to YM), VA Clinical Science and Rehabilitation R&D Awards (I01CX001388 and I01RX002604 to EC), and GE Healthcare. The authors acknowledge the scholarship support from the Joint Ph.D. Training Program of the University of Chinese Academy of Sciences to ZW.

Footnote

Conflicts of Interest: All authors have completed the ICMJE uniform disclosure form (available at https://dx.doi.org/10.21037/qims-21-308). JD serves as an unpaid editorial board member of *Quantitative Imaging in Medicine and Surgery*. The other authors have no other conflicts of interest to declare.

Ethical Statement: The authors are accountable for all aspects of the work in ensuring that questions related to the accuracy or integrity of any part of the work are appropriately investigated and resolved. The study was conducted in accordance with the Declaration of Helsinki (as revised in 2013).The study obtained ethics approval from the Institutional Review Board of University of California San Diego (No. 201647), and informed consent obtained from each subject.

References

1. Hoy D, March L, Woolf A, Blyth F, Brooks P, Smith E, Vos T, Barendregt J, Blore J, Murray C, Burstein R, Buchbinder R. The global burden of neck pain: Estimates from the global burden of disease 2010 study. Ann Rheum Dis 2014;73:1309-15.
2. Katz JN. Lumbar disc disorders and low-back pain: Socioeconomic factors and consequences. J Bone Joint Surg Am 2006;88:21-4.
3. An HS, Anderson PA, Haughton VM, Iatridis JC, Kang JD, Lotz JC, Natarajan RN, Oegema TR, Roughley P, Setton LA, Urban JP, Videman T, Andersson GBJ, Weinstein JN. Introduction. Disc degeneration: Summary. Spine (Phila Pa 1976) 2004;29:2677-8.
4. Peng B, Hou S, Wu W, Zhang C, Yang Y. The pathogenesis and clinical significance of a high-intensity zone (HIZ) of lumbar intervertebral disc on MR imaging in the patient with discogenic low back pain. Eur Spine J 2006;15:583-7.
5. Luoma K, Riihimäki H, Luukkonen R, Raininko R, Viikari-Juntura E, Lamminen A. Low back pain in relation to lumbar disc degeneration. Spine (Phila Pa 1976) 2000;25:487-92.
6. Bogduk N, Aprill C, Derby R. Lumbar discogenic pain: State-of-the-art review. Pain Med 2013;14:813-36.
7. Raj PP. Intervertebral Disc: Anatomy-Physiology-Pathophysiology-Treatment. Pain Pract 2008;8:18-44.
8. Antoniou J, Steffen T, Nelson F, Winterbottom N, Hollander AP, Poole RA, Aebi M, Alini M. The human lumbar intervertebral disc: Evidence for changes in the biosynthesis and denaturation of the extracellular matrix with growth, maturation, ageing, and degeneration. J Clin Invest 1996;98:996-1003.
9. Adams MA, Roughley PJ. What is intervertebral disc degeneration, and what causes it? Spine (Phila Pa 1976) 2006;31:2151-61.
10. Farshad-Amacker NA, Farshad M, Winklehner A, Andreisek G. MR imaging of degenerative disc disease. Eur J Radiol 2015;84:1768-76.
11. Cousins JP, Haughton VM. Magnetic resonance imaging of the spine. J Am Acad Orthop Surg 2009;17:22-30.
12. Mwale F, Iatridis JC, Antoniou J. Quantitative MRI as a diagnostic tool of intervertebral disc matrix composition and integrity. Eur Spine J 2008;17:432-40.
13. Hwang D, Kim S, Abeydeera NA, Statum S, Masuda K, Chung CB, Siriwanarangsun P, Bae WC. Quantitative magnetic resonance imaging of the lumbar intervertebral discs. Quant Imaging Med Surg 2016;6:744-55.
14. Wáng Y-XJ, Zhang Q, Li X, Chen W, Ahuja A, Yuan J. T1ρ magnetic resonance: basic physics principles and applications in knee and intervertebral disc imaging. Quant Imaging Med Surg 2015;5:858-85.
15. Nguyen AM, Johannessen W, Yoder JH, Wheaton AJ, Vresilovic EJ, Borthakur A, Elliott DM. Noninvasive quantification of human nucleus pulposus pressure with use of T1p-weighted magnetic resonance imaging. J Bone Joint Surg Am 2008;90:796-802.
16. Johannessen W, Auerbach JD, Wheaton AJ, Kurji A, Borthakur A, Reddy R, Elliott DM. Assessment of human disc degeneration and proteoglycan content using T1ρ-weighted magnetic resonance imaging. Spine (Phila Pa 1976) 2006;31:1253-7.
17. Blumenkrantz G, Li X, Han ET, Newitt DC, Crane JC, Link TM, Majumdar S. A feasibility study of in vivo T1ρ imaging of the intervertebral disc. Magn Reson Imaging 2006;24:1001-7.
18. Zhou Z, Jiang B, Zhou Z, Pan X, Sun H, Huang B, Liang T, Ringgaard S, Zou X. Intervertebral disk degeneration : T1ρ MR imaging of human and animal models. Radiology 2013;268:492-500.
19. Vadalà G, Russo F, Battisti S, Stellato L, Martina F, Vescovo RD, Giacalone A, Borthakur Arijitt, Zobel BB, Denaro V. Early Intervertebral Disc Degeneration Changes in Asymptomatic Weightlifters Assessed by T1ρ-Magnetic Resonance Imaging. Spine (Phila Pa 1976) 2014;39:1881-6.
20. Zhang Y, Hu J, Duan C, Hu P, Lu H, Peng X. Correlation study between facet joint cartilage and intervertebral discs in early lumbar vertebral degeneration using T2, T2* and T1ρ mapping. PLoS One 2017;12:e0178406.
21. Wang YXJ, Zhao F, Griffith JF, Mok GSP, Leung JCS, Ahuja AT, Yuan J. T1rho and T2 relaxation times for lumbar disc degeneration: An in vivo comparative study at 3.0-Tesla MRI. Eur Radiol 2013;23:228-34.
22. Yoon MA, Hong SJ, Kang CH, Ahn KS, Kim BH. T1rho and T2 mapping of lumbar intervertebral disc: Correlation with degeneration and morphologic changes in different disc regions. Magn Reson Imaging 2016;34:932-9.
23. Ling Z, Li L, Chen Y, Hu H, Zhao X, Wilson J, Qi Q, Liu D, Wei F, Chen X, Lu J, Zhou Z, Zou X. Changes of the end plate cartilage are associated with intervertebral disc degeneration: A quantitative magnetic resonance imaging study in rhesus monkeys and humans. J Orthop Translat 2020;24:23-31.
24. Fields AJ, Han M, Krug R, Lotz JC. Cartilaginous end

plates: Quantitative MR imaging with very short echo times-orientation dependence and correlation with biochemical composition. Radiology 2015;274:482-9.
25. Ma YJ, Carl M, Searleman A, Lu X, Chang EY, Du J. 3D adiabatic T1ρ prepared ultrashort echo time cones sequence for whole knee imaging. Magn Reson Med 2018;80:1429-39.
26. Bae WC, Statum S, Zhang Z, Yamaguchi T, Wolfson T, Gamst AC, Du, J, Bydder, GM, Masuda, K, Chung CB. Morphology of the cartilaginous endplates in human intervertebral disks with ultrashort echo time MR imaging. Radiology 2013;266:564-74.
27. Hänninen N, Rautiainen J, Rieppo L, Saarakkala S, Nissi MJ. Orientation anisotropy of quantitative MRI relaxation parameters in ordered tissue. Sci Rep 2017;7:9606.
28. Wu M, Ma Y, Kasibhatla A, Chen M, Jang H, Jerban S, Chang EY, Du J. Convincing evidence for magic angle less-sensitive quantitative T1ρ imaging of articular cartilage using the 3D ultrashort echo time cones adiabatic T1ρ(3D UTE cones-AdiabT1ρ) sequence. Magn Reson Med 2020;84:2551-60.
29. Wu M, Ma Y, Wan L, Jerban S, Jang H, Chang EY, Du J. Magic angle effect on adiabatic T1ρ imaging of the Achilles tendon using 3D ultrashort echo time cones trajectory. NMR Biomed 2020;33:e4322.
30. Wang L, Han M, Wong J, Zheng P, Lazar AA, Krug R, Fields AJ. Evaluation of human cartilage endplate composition using MRI: Spatial variation , association with adjacent disc degeneration , and in vivo repeatability. J Orthop Res 2021;39:1470-8.
31. Law T, Anthony MP, Chan Q, Samartzis D, Kim M, Cheung KMC, Khong PL. Ultrashort time-to-echo MRI of the cartilaginous endplate: Technique and association with intervertebral disc degeneration. J Med Imaging Radiat Oncol 2013;57:427-34.
32. Gurney PT, Hargreaves BA, Nishimura DG. Design and analysis of a practical 3D cones trajectory. Magn Reson Med 2006;55:575-82.
33. Periaswamy S, Farid H. Elastic registration in the presence of intensity variations. IEEE Trans Med Imaging 2003;22:865-74.
34. Wu M, Zhao W, Wan L, Kakos L, Li L, Jerban S, Jang H, Chang EY, Du J, Ma YJ. Quantitative three-dimensional ultrashort echo time cones imaging of the knee joint with motion correction. NMR Biomed 2020;33:e4214.
35. Griffith JF, Wang YXJ, Antonio GE, Choi KC, Yu A, Ahuja AT, Leung PC. Modified Pfirrmann grading system for lumbar intervertebral disc degeneration. Spine (Phila Pa 1976) 2007;32:E708-12.
36. Akella SVS, Regatte RR, Gougoutas AJ, Borthakur A, Shapiro EM, Kneeland JB, Leigh JS, Reddy R. Proteoglycan-induced changes in T1ρ-relaxation of articular cartilage at 4T. Magn Reson Med 2001;46:419-23.
37. Cao Y, Guo Q wei, Wan Y. Significant Association between the T2 Values of Vertebral Cartilage Endplates and Pfirrmann Grading. Orthop Surg 2020;12:1164-72.
38. Sharafi A, Xia D, Chang G, Regatte RR. Biexponential T1ρ relaxation mapping of human knee cartilage in vivo at 3T. NMR Biomed 2017;30:10.1002/nbm.3760.
39. Lustig M, Donoho D, Pauly JM. Sparse MRI: The application of compressed sensing for rapid MR imaging. Magn Reson Med 2007;58:1182-95.
40. Wu Y, Ma Y, Liu J, Du J, Xing L. Self-attention convolutional neural network for improved MR image reconstruction. Inf Sci (N Y) 2019;490:317-28.

Cite this article as: Wei Z, Lombardi AF, Lee RR, Wallace M, Masuda K, Chang EY, Du J, Bydder GM, Yang W, Ma YJ. Comprehensive assessment of *in vivo* lumbar spine intervertebral discs using a 3D adiabatic $T_{1\rho}$ prepared ultrashort echo time (UTE-Adiab-$T_{1\rho}$) pulse sequence. Quant Imaging Med Surg 2022;12(1):269-280. doi: 10.21037/qims-21-308

Numerical simulations

Numerical simulations were conducted to choose appropriate pulse sequence parameters for the in vivo study. Nominal T_1 and $T_{1\rho}$ values were set at 1200 ms and 100 ms, respectively. First, the flip angle (FA) was fixed at 6° and the repetition time (TR) at 2000 ms, and then data was acquired with 12 different number of spokes (i.e., Nsp). Values of Nsp ranged from 1 to 56 with an interval of 5 between. Simulation results showed that 41 was the optimal Nsp. Second, with the Nsp fixed at 41 as well as FA, T_1 and $T_{1\rho}$ values unchanged, TRs were set at 1600 to 3600 ms with an interval of 400 ms between them. With each simulation, $T_{1\rho}$ weighted signals were generated with four different spin lock times (TSLs) (i.e., 0, 24, 48, 72 ms).

Under different parameter combinations, magnetic resonance (MR) signals were generated by Bloch equation simulation. $T_{1\rho}$ values were calculated by fitting the simulated signals with the following equation:

$$S(TSL) = S_0 e^{-\frac{TSL}{T_{1\rho}}} + C \quad [1]$$

where S_0 is the initial signal intensity, and the constant C is included to accommodate non-$T_{1\rho}$ related signals, such as the background noise and artifacts generated during data acquisition and image reconstruction.

Simulation results are shown in *Figure S1*, where we found that Nsp=41 and TR = 2000 ms are the optimal parameters showing the smallest $T_{1\rho}$ errors.

To reduce the scan time for the in vivo study, a relatively large value of Nsp (i.e., 41) together with a relatively short TR (i.e., 2000ms) were used in this study. Both multispoke data acquisition and reduced TR (less than five times the tissue T_1) will lead to T_1 weighting. In our simulation, we found that the $T_{1\rho}$ fitting error due to T_1 contamination could be partially compensated for by adjustment of Nsp. Multispoke data acquisition and reduced TR affect the $T_{1\rho}$ fitting in opposite ways. An optimized Nsp could potentially be obtained to minimize the $T_{1\rho}$ quantification error for a particular tissue.

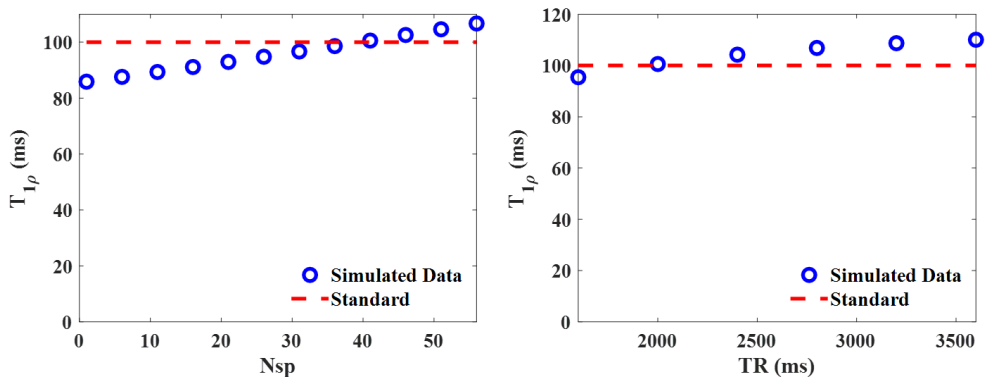

Figure S1 $T_{1\rho}$ values simulated with different Nsps (left) and different TRs (right). The red dashed line is the nominal $T_{1\rho}$ value (100 ms) and the blue circles are the simulated $T_{1\rho}$ values. Nsp: number of spokes; TR: repetition time.

https://dx.doi.org/10.21037/qims-21-308

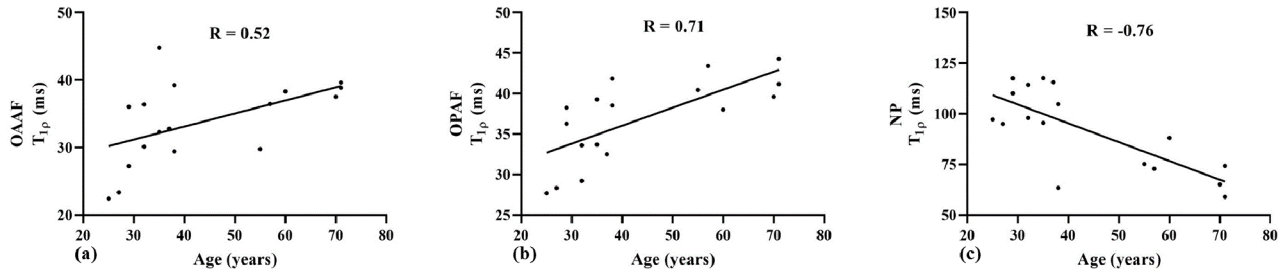

Figure S2 Scatter plots for the $T_{1\rho}$ values of OAAF, OPAF, and NP as a function of age. (a) is the correlation between $T_{1\rho}$ of OAAF and age; (b) is the correlation between $T_{1\rho}$ of OPAF and age; (c) is the correlation between $T_{1\rho}$ of the NP and age. OAAF: outer anterior annulus fibrosus (AF); OPAF: outer posterior AF; NP: nucleus pulposus.

Table S1 $T_{1\rho}$ value (mean and standard deviation) of each intervertebral disc sub-region for each modified Pfirrmann grade group. The grades increase from group 1 to group 4

Group	Grade	Disc Counts	$T_{1\rho}$ (ms)						
			OAAF	IAAF	OPAF	IPAF	SCEP	ICEP	NP
Group 1	2	31 (36.5%)	33.2±7.8	44.9±7.7	34.0±5.0	45.4±6.5	36.0±5.0	36.9±3.9	118.7±10.9
Group 2	3	21 (24.7%)	32.8±6.6	44.4±6.8	34.7±4.5	46.0±7.5	38.6±6.3	39.1±5.2	94.7±12.2
	4								
Group 3	5	18 (21.2%)	34.6±6.7	44.9±4.6	40.8±7.2	47.5±6.3	38.8±3.8	39.9±3.3	71.2±5.1
	6								
Group 4	7	15 (17.6%)	35.8 ±5 8	42.8±5.8	41.0±5.1	47.3±7.0	42.7±4.6	42.1±4.9	57.9±8.1
	8								

OAAF: outer anterior annulus fibrosus (AF); IAAF: inner anterior AF; OPAF: outer posterior AF; IPAF: inner posterior AF, SCEP: superior cartilaginous endplate (CEP); ICEP: inferior CEP; NP: nucleus pulposus.

https://dx.doi.org/10.21037/qims-21-308

Table S2 P values of $T_{1\rho}$ value differences between every pair of groups analyzed with the ANOVA method in each sub-region. P<0.05, significant difference

Group OAAF		P						
		IAAF	OPAF	IPAF	SCEP	ICEP	NP	
Group 1	Group 2	0.846	0.816	0.648	0.763	0.077	0.073	0.000
	Group 3	0.497	0.973	0.000	0.312	0.068	0.020	0.000
	Group 4	0.235	0.329	0.000	0.391	0.000	0.000	0.000
Group 2	Group 1	0.846	0.816	0.648	0.763	0.077	0.073	0.000
	Group 3	0.425	0.813	0.001	0.503	0.898	0.560	0.000
	Group 4	0.205	0.474	0.001	0.584	0.020	0.046	0.000
Group 3	Group 1	0.497	0.973	0.000	0.312	0.068	0.020	0.000
	Group 2	0.425	0.813	0.001	0.503	0.898	0.560	0.000
	Group 4	0.619	0.364	0.888	0.931	0.033	0.158	0.000
Group 4	Group 1	0.235	0.329	0.000	0.391	0.000	0.000	0.000
	Group 2	0.205	0.474	0.001	0.584	0.020	0.046	0.000
	Group 3	0.619	0.364	0.888	0.931	0.033	0.158	0.000

OAAF: outer anterior annulus fibrosus (AF); IAAF: inner anterior AF; OPAF: outer posterior AF; IPAF: inner posterior AF, SCEP: superior cartilaginous endplate (CEP); ICEP: inferior CEP; NP: nucleus pulposus.

https://dx.doi.org/10.21037/qims-21-308